Fractionation in Gay-Berne liquid crystal mixtures

J. Antonio Moreno-Razo and Enrique Díaz-Herrera
Departamento de Física, Universidad Autónoma Metropolitana-Iztapalapa, Mexico, D.F., Mexico

Sabine H. L. Klapp*
Stranski-Laboratorium für Physikalische und Theoretische Chemie, Sekretariat C7, Technische Universität Berlin, Strasse des 17, Juni 115, D-10623 Berlin, Germany
and Institut für Theoretische Physik, Sekretariat PN 7-1, Technische Universität Berlin, Hardenbergstrasse 36, D-10623 Berlin, Germany

(Received 23 April 2007; revised manuscript received 5 July 2007; published 9 October 2007)

We present a constant-pressure molecular dynamics simulation study of the phase behavior of binary (50:50) Gay-Berne liquid crystal mixtures consisting of elongated particles with different lengths ($L_A > L_B$) and equal diameters. We focus on systems at dense liquid-state conditions. Considering three mixtures characterized by different values of $L_{A(B)}$ and different length ratios $q = L_B/L_A < 1$, we find complex fluid-fluid phase behavior resulting from the interplay between nematic, smectic-*A*-type, or smectic-*B*-type orientational ordering, on the one hand, and demixing into two phases of different composition (fractionation), on the other hand. The driving "forces" of demixing transitions are the temperature and the length ratio. Indeed, in the system characterized by the largest value of q ($q=0.86$) orientational order occurs already in *mixed* states, whereas full fractionation is found at $q=0.71$. The two resulting states are either of type smectic-*B*-nematic (intermediate temperatures) or smectic-*B*-smectic-*B* (low temperatures). In the intermediate case $q=0.80$ we observe a stepwise ordering and demixing behavior on cooling the system from high temperatures. Moreover, our results show that the stability range of (partially) nematic structures in mixtures of sufficiently small q can be significantly larger than in the pure counterparts, in qualitative agreement with experimental observations.

DOI: 10.1103/PhysRevE.76.041703 PACS number(s): 64.70.Md, 61.20.Ja

I. INTRODUCTION

Since their discovery more than a century ago [1–4] liquid crystals (LC) have always been a subject of intense research both experimentally and theoretically [5], stimulated also by the wide range of (device) applications of such systems, e.g., in LC displays. From a statistical-physics point of view, the phase behavior of liquid crystals serves as a key example of entropically driven phase transitions. Indeed, as shown by Onsager [6] already in 1949, the isotropic-nematic transition in systems of (infinitely) long and thin rods can be explained as a result of a competition between translational and rotational entropy. Later, computer simulations have played a decisive role in understanding the complex phase behavior of LC systems (see, e.g., Refs. [7–10]), especially when it comes to the role of molecular shape, attractive interactions and/or multipolar forces arising, e.g., from ions or dipole moments [11].

In the present paper we report molecular dynamics (MD) computer simulations of the phase behavior of LC model *mixtures*, focusing on the ordering behavior of systems of particles with different lengths L_a (with a being the species index) and equal diameters D_a. From a practical point of view, one main motivation to study such systems is that their enriched phase behavior relative to the monodisperse case makes them more suitable for device applications. An important example is the growth of the nematic phase region observed in experiments of binary [12] and ternary [13] (organic) LC mixtures (thermotropic liquid crystals). In these systems, the temperature related to nematic-smectic transitions is significantly reduced compared to the one-component case, that is, the onset of orientational order combined with partial (one-dimensional) translational order is delayed. Similarly, Lopez *et al.* [14] found a growth of the smectic-*A* region and an accompanying depression of more ordered phases in organic LC mixtures of 8CB and 8OCB. Further studies on compounds of organic molecules have been performed by Naoum *et al.* (see Ref. [15] and references therein). On the other hand, length dispersity also occurs in colloidal suspensions of *mesoscopic* rods with lengths in the nanometer-to-micrometer range and much larger length-to-breadth ratios $\kappa_a = L_a/D_a$ compared to the organic molecules. Examples are boehmite needles [16,17] and carbon nanotubes [18]. For such systems one is typically interested in *fractionation*, that is, the occurrence of demixing phase transitions of the mixed fluid system into subphases dominated by a specific length. Understanding the conditions of fractionation may help to deliberately purify colloidal rod suspensions, e.g., by compression. Interestingly, fractionation has rarely been reported in the experimental studies of the organic LC mixtures mentioned before [12–15]; indeed, these studies rather focused on the *overall* phase behavior (as a function of concentration) rather than on species-resolved properties.

Theoretical research on LC mixtures of elongated particles focuses on hard-core systems, starting with the work of Leckerkerker and co-workers [16,19–21] who investigated *binary* mixtures of hard rods of different lengths L_A and $L_B < L_A$. Based on Onsager theory it was found that the isotropic-nematic transition of such mixtures is coupled with

*sabine.klapp@fluids.tu-berlin.de

fractionation for sufficiently small values of the length ratios $q=L_B/L_A \leq 1$. These findings have been supported by a recent Monte Carlo (MC) simulation study of *polydisperse* hard rod mixtures [22] which also display isotropic-nematic transitions combined with demixing. Further MC studies on (binary) hard-particle mixtures with different lengths have been concerned with the order parameters at the isotropic-nematic transition [23] and the isotropic-nematic coexistence in the Lebwohl-Lasher (lattice) mixture model [24]. On the other hand, density-functional methods have been employed to investigate features of the nematic-smectic-*A* transition [25] and fractionation within the smectic phase [26,27]. We also note that there is a large amount of theoretical and experimental work on the related case of binary mixtures of thin and thick hard rods, i.e., $D_A \neq D_B$, $L_A=L_B$ [28–31].

The present paper concerns systems with *attractive* interactions in addition to the anisotropic steric ones. Compared to hard-core LC systems, the understanding of attractive mixtures is less developed, although presence of such interactions is rather the rule than an exception. In molecular (organic) LC compounds attractive interactions usually result from van der Waals (induced dipole-dipole) interactions and from asymmetric charge distributions yielding multipoles such as permanent dipole moments embedded in the molecules. An immediate effect of such attractive interactions is temperature dependence of the LC phase behavior, which has first been described theoretically by Maier and Saupe [32]. The van der Waals interactions may also be relevant in colloidal rod suspensions, where additional attractions may arise from the (entropy-induced) depletion effect, that is, the fact that nearby rods form an effective excluded volume for the solvent molecules. A standard model incorporating attractive (van der Waals) interactions in small elongated molecules is the Gay-Berne (GB) model [33], a modification of the usual Lennard-Jones potential for spherical molecules. Compared to purely repulsive LC particles, one important effect of attraction in one-component GB systems is the stabilization of smectic relative to nematic phases, as has been demonstrated in extensive simulation studies [34,35] for a broad range of length-to-breadth ratios. The GB potential has been recently generalized for mixtures [36], opening the way for several computer simulation studies by Cleaver *et al.* [37–39] on the phase behavior of such systems. One main topic of these studies was to which extent the GB models can reproduce the experimentally observed broadening of the nematic range.

In the present study we focus on yet a different aspect of the GB mixture phase behavior, namely the conditions under which *demixing* phase transitions (fractionation) occur. In view of the large space spanned by the various geometric and energetic parameters defining a GB mixture, it is clear that such a study must be restricted to some representative examples. Here we consider three systems characterized by different values of length-to-breadth ratios $\kappa_{A(B)}$ and different length ratios $q<1$. In order to make contact to already existing data we employ the same model parameters previously considered by Cleaver *et al.* [37–39]. However, the latter studies focus on densities (or pressures, respectively) typical for nematic states. In the present work we explore the system's behavior in the *smectic range* at which the nematic phase of the pure systems is unstable. Our results demonstrate that this gives rise to qualitative effects. Technically, we investigate the systems via constant-pressure MD simulations [40]. This method has turned out to be particularly useful to investigate demixing transitions in our earlier studies of "simple" mixtures consisting of spherical particles [41–43].

The rest of the paper is organized as follows. In Sec. II we present the model and describe some details of the *NPT*-MD simulations employed in this work. Numerical results are given in Sec. III where we start with a brief discussion of pure GB fluids with $\kappa=3.0$ and attraction parameters $\nu=2$, $\mu=1$ (Sec. III A). We then explore the phase behavior of the three mixtures I–III characterized by an increasing degree of bidispersity (Secs. III B–III D). Finally, our conclusions are summarized in Sec. IV.

II. MODEL AND SIMULATION DETAILS

A. Pair potential

We consider binary (50:50) mixtures of two species *A* and *B* of rigid ellipsoidal molecules with different lengths $L_A > L_B$ and equal breadths $D_A=D_B$. The molecules interact via the two-component generalization [36] of the standard GB potential [33] which involves both repulsive and attractive parts. Specifically, the GB interaction between two particles *i* and *j* with center-of-mass positions $\mathbf{r}_i$, $\mathbf{r}_j$ and orientation unit vectors $\mathbf{u}_i$, $\mathbf{u}_j$ is given by

$$U_{ab}^{\mathrm{GB}}(\hat{\mathbf{r}}_{ij},\mathbf{u}_i,\mathbf{u}_j) = 4\epsilon_{ab}(\hat{\mathbf{r}}_{ij},\mathbf{u}_i,\mathbf{u}_j)(\bar{R}_{ij}^{-12}-\bar{R}_{ij}^{-6}), \tag{2.1}$$

where $\hat{\mathbf{r}}_{ij}=\mathbf{r}_{ij}/r_{ij}$ is a unit vector along the center-to-center vector $\mathbf{r}_{ij}=\mathbf{r}_i-\mathbf{r}_j$, $r_{ij}=|\mathbf{r}_{ij}|$ is the particle separation, and the subscripts *a* and *b* denote the mixture components considered $[a(b)=A,B]$. Furthermore, the scaled distance $\bar{R}_{ij}$ is given by

$$\bar{R}_{ij} = \frac{1}{\sigma_0}[r_{ij}-\sigma_{ab}(\hat{\mathbf{r}}_{ij},\mathbf{u}_i,\mathbf{u}_j)+\sigma_0], \tag{2.2}$$

where $\sigma_{ab}(\hat{\mathbf{r}}_{ij},\mathbf{u}_i,\mathbf{u}_j)$ is the generalized range parameter defining the distance at which the potential vanishes, that is

$$\sigma_{ab}(\hat{\mathbf{r}}_{ij},\mathbf{u}_i,\mathbf{u}_j) = \sigma_0\left[1-\frac{\chi_{ab}}{2}\left(\frac{(\alpha_{ab}\mathbf{u}_i\cdot\hat{\mathbf{r}}_{ij}+\alpha_{ab}^{-1}\mathbf{u}_j\cdot\hat{\mathbf{r}}_{ij})^2}{1+\chi_{ab}\mathbf{u}_i\cdot\mathbf{u}_j} + \frac{(\alpha_{ab}\mathbf{u}_i\cdot\hat{\mathbf{r}}_{ij}-\alpha_{ab}^{-1}\mathbf{u}_j\cdot\hat{\mathbf{r}}_{ij})^2}{1-\chi_{ab}\mathbf{u}_i\cdot\mathbf{u}_j}\right)\right]^{-1/2}. \tag{2.3}$$

In Eq. (2.3),

$$\chi_{ab} = \sqrt{\frac{(L_a^2-D_a^2)(L_b^2-D_b^2)}{(L_b^2+D_a^2)(L_a^2+D_b^2)}}, \tag{2.4}$$

is the generalization of the usual χ parameter appearing in the one-component GB model [33], and α_{ab} is a new parameter needed in the binary version to distinguish between the two nonequivalent teelike configurations where the top of a $B(A)$ ellipsoid touches the equator of an $A(B)$ ellipsoid [36]. Specifically,

TABLE I. Geometric parameters characterizing the mixtures considered in this work ($\kappa_a = L_a/D_a = L_a/\sigma_0$, $q = L_B/L_A$).

System	κ_A	κ_B	q
I	3.5	3.0	0.86
II	2.5	2.0	0.80
III	4.2	3.0	0.71

$$\alpha_{ab}^2 = \sqrt{\frac{(L_a^2 - D_a^2)(L_b^2 + D_a^2)}{(L_b^2 - D_b^2)(L_a^2 + D_b^2)}}. \tag{2.5}$$

From Eq. (2.5) one can see that α_{ab} smoothly approaches unity in the one-component limit (i.e., $L_A \to L_B$, $D_A \to D_B$). In the present work we set the diameters D_a equal to the length σ_0 appearing in the range function [see Eqs. (2.2) and (2.3)].

Finally, the interaction strength $\epsilon_{ab}(\hat{\mathbf{r}}_{ij}, \mathbf{u}_i, \mathbf{u}_j)$ also depends on the relative orientation of the molecules and takes the form

$$\epsilon_{ab}(\hat{\mathbf{r}}_{ij}, \mathbf{u}_i, \mathbf{u}_j) = \epsilon_{ab} \epsilon_{1,ab}^{\nu}(\mathbf{u}_i, \mathbf{u}_j) \epsilon_{2,ab}^{\mu}(\hat{\mathbf{r}}_{ij} \mathbf{u}_i, \mathbf{u}_j), \tag{2.6}$$

where the parameters ϵ_{ab} characterize the depths of the a-b attraction wells. As to the functions $\epsilon_{1,ab}^{\nu}$ and $\epsilon_{2,ab}^{\mu}$ appearing on the right-hand side of Eq. (2.6), ν and μ are adjustable exponents, and the functions are defined as [36]

$$\epsilon_{1,ab}^{\nu}(\mathbf{u}_i, \mathbf{u}_j) = [1 - \chi_{ab}^2 (\mathbf{u}_i \cdot \mathbf{u}_j)^2]^{-\nu/2} \tag{2.7}$$

and

$$\epsilon_{2,ab}^{\mu}(\hat{\mathbf{r}}_{ij}, \mathbf{u}_i, \mathbf{u}_j) = \left[1 - \frac{\chi'_{ab}}{2} \left(\frac{(\alpha'_{ab} \mathbf{u}_i \cdot \hat{\mathbf{r}}_{ij} + \alpha'^{-1}_{ab} \mathbf{u}_j \cdot \hat{\mathbf{r}}_{ij})^2}{1 + \chi'_{ab} \mathbf{u}_i \cdot \mathbf{u}_j} + \frac{(\alpha'_{ab} \mathbf{u}_i \cdot \hat{\mathbf{r}}_{ij}) - \alpha'^{-1}_{ab} \mathbf{u}_j \cdot \hat{\mathbf{r}}_{ij})^2}{1 - \chi'_{ab} \mathbf{u}_i \cdot \mathbf{u}_j} \right) \right]^{\mu}. \tag{2.8}$$

In Eq. (2.8), the parameters χ'_{ab} are defined as

$$\chi'_{ab} = (\kappa'^{1/\mu}_{ab} - 1)/(\kappa'^{1/\mu}_{ab} + 1) \tag{2.9}$$

with $\kappa'_{ab} = \epsilon^s_{ab}/\epsilon^e_{ab}$, where ϵ^s_{ab} is the depth of the attractive potential well for an a-b pair of particles oriented parallel side-by-side, and ϵ^e_{ab} is the corresponding depth for a pair of particles oriented end-to-end. Finally, the (free) parameters α'_{ab} are introduced [36] in order to distinguish between the attractive interactions related to the two nonequivalent tee configurations [in analogy to the previously introduced parameters α_{ab} involved in the range function, see Eqs. (2.3) and (2.5)].

In the present work we consider three different mixtures I, II, and III differing in the length-to-breadth ratios $\kappa_a = L_a/D_a = L_a/\sigma_0$ (with $a = A, B$), and in the length ratios $q = L_B/L_A < 1$. A summary of the geometric parameters employed is given in Table I; the remaining (energetic) model parameters are presented in the Appendix. As seen from Table I, Mixture II falls somewhat out of the series in that the length-to-breadth ratios κ_a are significantly smaller than in the other systems. The main reason for choosing this particular system (rather than a system with $\kappa_A = 3.8$ and $\kappa_B = 3.0$, which would lead to nearly the same value of q) is that there are earlier simulation results (based on the Gibbs-ensemble Monte Carlo method) [38] where, however, the characteristics of demixing phenomena were not fully discussed. We therefore decided to first investigate in more detail this system before proceeding to yet a different mixture for which, so far, no results exist. The same reasoning applies to the parameter choices for mixtures I and III which have been previously employed in Refs. [37] and [39], respectively. These latter studies explore, however, the phase behavior at high pressures (typical for nematic states), whereas the present study focuses on low-pressure orientational states.

B. Molecular dynamics simulations

The MD simulations were carried out in a *NPT* ensemble, where the temperature T and pressure P were fixed using a Nosé-Hoovers thermostat and barostat, respectively [40], and the particle number $N = 1372$. To detect any system size dependence some additional runs with $N = 4000$ were done at particularly interesting state points. The simulations were started from mixed, orientationally isotropic face-centered-cubic crystals, where the two species were randomly distributed on the lattice sites and randomly oriented. Low-temperature states were usually found by a stepwise cooling of the system. However, in order to be sure that the resulting states do not depend on the initial configurations, we have also performed various test simulation at low T, where we started directly from randomly oriented high-temperature states. The initial velocities of the molecules were chosen from a Maxwell-Boltzmann distribution, and the moments of inertia were set to $I_a = (\sigma_0^2/20)(\kappa_a^2 + 1)$ [44] (with the masses set to unity). The translational and rotational equations of motion were integrated using the velocity-Verlet algorithm [40] with a reduced time step $\delta t^* = (\epsilon_{BB}/\sigma_0^2)^{1/2}$, $t = 1.5 \times 10^{-3}$. We used tetragonal boxes with (mutually orthogonal) box sides L_x, L_y, and L_z. In the *NPT* simulations of spatially homogeneous (i.e., isotropic or nematic states we restricted the box sides to vary equally, that is, we set $L_\gamma = L$ ($\gamma = x, y, z$). On the other hand, in smectic phases (which are characterized by one-dimensional translational ordering) we allowed the box sides to change independently, which turned out to be important to find the true equilibrium state. In all cases, the simulation box was periodically replicated along the x, y, and z directions.

To save computational time the intermolecular potentials were truncated (independently of the species considered) at $r_c = (\kappa_{\max} + 1)\sigma_0$, where $\kappa_{\max} = \kappa_A$ is the length-to-breadth ratio of the longer (A) particles.

Typical runs then consisted of at least three-million time steps for equilibration, followed by a production period of similar length. To minimize correlations between measurements we calculated thermodynamic and structural quantities every 50 time steps.

C. Characterization of the ordered phases

The degree of orientational ordering in the GB mixtures was monitored via the second-rank order parameter P_2 defined in the usual way [40] as the largest eigenvalue of the

ordering matrix $\mathbf{Q}=(1/N)\Sigma_{i=1}^{N}(3\mathbf{u}_i\mathbf{u}_i-\mathbf{I})/2$, where $\mathbf{I}$ is the identity matrix. The corresponding normalized eigenvector is the global director $\mathbf{n}$. To characterize the translational and orientational structure within the individual phases we have calculated various pair correlation functions. In particular, to detect the appearance of smectic ordering (that is, arrangement of the molecules into layers) of species a, we consider the functions

$$g_{\parallel}^{aa}(r_{\parallel})=\frac{\left\langle \sum_{i\neq j}^{N_a}\delta(r_{\parallel}-r_{ij,\parallel})\,\theta(\sigma_0/2-r_{ij,\perp})\right\rangle}{2N_a\rho_a\pi(\sigma_0/2)^2\Delta r}, \quad (2.10)$$

where $\theta(x)$ is the step function, $r_{ij,\parallel}=|\mathbf{r}_{ij,\parallel}|=|\mathbf{r}_{ij}\cdot\mathbf{n}|$ is the separation between the centers of masses along the nematic director and $r_{ij,\perp}=|\mathbf{r}_{ij,\perp}|=|\mathbf{r}_{ij}-\mathbf{r}_{ij,\parallel}|$ is the corresponding transversal separation (note that our definition involves only pairs of molecules in a cylinder of diameter equal to the breadth of a molecule, σ_0). Also, $\Delta r=0.05\sigma_0$ is a tolerance, and the factor 2 in the denominator arises due to the symmetry $\mathbf{r}_{ij,\parallel}\rightarrow-\mathbf{r}_{ij,\parallel}$. Smectic (Sm) layering is signaled by (essentially undamped) oscillations in $g_{\parallel}^{aa}(r_{\parallel})$, with the period of these oscillations indicating the layer spacing. In nematic (N) states, on the other hand, $g_{\parallel}^{aa}(r_{\parallel})$ has rather liquidlike (i.e., short-ranged) structure.

The translational structure of species a within a layer (if present) is monitored via the quasi-two-dimensional pair distributions

$$g_{\perp}^{aa}(r_{\perp})=\frac{\left\langle \sum_{i\neq j}^{N_a}\delta(r_{\perp}-r_{ij,\perp})\,\theta(L_a/2-r_{ij,\parallel})\right\rangle}{2N_a\rho_a\pi r\Delta r L_a}, \quad (2.11)$$

which involves only particles in a disk of height L_a around a given particle. In smectic-A (Sm_A) states, $g_{\perp}^{aa}(r_{\perp})$ has short-ranged structure only indicating the liquidlike distribution of the particles within the layer. On the other hand, smectic-B (Sm_B) phases are characterized by a pronounced and rather long-ranged structure of $g_{\perp}^{aa}(r_{\perp})$ resembling that observed in crystalline configurations with hexagonal structure. A typical feature of such arrangements is the splitting of the second peak into two subpeaks.

A further indication for Sm_B-like ordering is the presence of interlayer correlations, particularly the transverse shift of a particle in an adjacent layer relative to its nearest neighbor in the layer considered due to the local hexagonal ordering. These correlations may be detected from the functions [45]

$$g_{\perp}'^{aa}(r_{\perp})=\frac{\left\langle \sum_{i\neq j}^{N_a}\delta(r_{\perp}-r_{ij,\perp})\right\rangle}{N_a\rho_a\pi\Delta r L_a}, \quad (2.12)$$

which, contrary to $g_{\perp}^{aa}(r_{\perp})$ defined in Eq. (2.11), involve *all* pairs of particles of species a (therefore, many different values of $r_{ij,\parallel}$). As a consequence, $g_{\perp}'^{aa}(r_{\perp})$ does not necessarily go to zero for $r_{\perp}\rightarrow 0$ as it is the case for $g_{\perp}^{aa}(r_{\perp})$.

Finally, to detect any *demixing* of the A and B particles in the simulation box we have monitored the density profiles

$$\rho_a(z)=\frac{\langle N_a(\gamma)\rangle}{A_{\gamma}h}, \quad (2.13)$$

where γ is the Cartesian direction considered ($\gamma=x,y,z$), A_{γ} is the box area orthogonal to this direction, and $N_a(\gamma)$ is the number of particles of species a in a thin slice of width $\Delta\gamma=0.02\sigma_0$.

III. RESULTS

All simulations of the present work have been performed at fixed reduced pressures $P^*=P\sigma_0^3/\epsilon_{BB}$ typical for liquid states (if not otherwise stated, $P^*=0.5$). The system's phase behavior is then explored by varying the reduced temperature $T^*=k_BT/\epsilon_{BB}$ (with k_B being Boltzmann's constant). Typically we have used temperature steps of $\delta T^*=0.01$.

A. Background: Pure GB fluid with $\kappa=3.0$

As a background for our later discussion of the GB mixtures it is useful to briefly discuss the behavior of dense, *one-component* GB fluids. We take particles characterized by the length-to-breadth ratio $\kappa=3.0$ as a representative example. This case has been extensively discussed in the literature (see, e.g., Refs. [34,35]), but most of these studies have been performed with other values (compared to ours) for the exponents characterizing the interaction strength [see Eqs. (2.8) and (2.7)], namely the values $\nu=1$ and $\mu=2$ suggested in the original work of Gay and Berne [33]. Results for the present choice $\nu=2$, $\mu=1$ (and $\kappa=3.0$) are, so far, not available. It is therefore important to clarify the role of the exponents on the phase behavior.

With the previously investigated choice $\nu(\mu)=1(2)$, the phase diagram at $\kappa=3.0$ [34,35] involves an isotropic (I) phase with a gas-liquid critical point at low reduced densities ($\rho^*=N\sigma_0^3/V\lesssim 0.25$) and a Sm_B phase at high densities ($\rho^*\gtrsim 0.3$). For sufficiently high temperatures (and not too high densities) an additional nematic (N) phase appears in between the isotropic and the Sm_B phase. There is no Sm_A phase at this particular elongation, indeed, such phases only become stable at higher elongations, such as $\kappa=3.6$ [35]. For the latter systems one observes an "island" of Sm_A states in between the nematic and Sm_B phase region.

In the present work we set $\nu=2$ (and $\mu=1$), implying an enhanced attraction in parallel configurations of two GB molecules [see Eq. (2.7)]. In order to explore the effect on the phase behavior, particularly the anisotropic phases, we present in Fig. 1 results for the order parameter P_2 as a function of T^* for the two pressures $P^*=0.5$ and $P^*=1.0$. Corresponding data for the average densities $\rho^*=N\sigma_0^3/\langle V\rangle$ and internal energies $U^*=U/\epsilon_{BB}N$ are plotted in the two parts of Fig. 2. We first consider the ordering behavior at $P^*=0.5$. At temperatures $T^*\gtrsim 1.0$ the system is isotropic as indicated by the very small values of $P_2\lesssim 0.1$ (note that small nonzero values of P_2 are expected even in disordered states due to the finite size of the simulation system [46]). Upon cooling from this isotropic state, one observes a pronounced "jump" of P_2 toward a large nonzero value at $T^*\approx 1.0$, followed by a second, smaller jump directly below

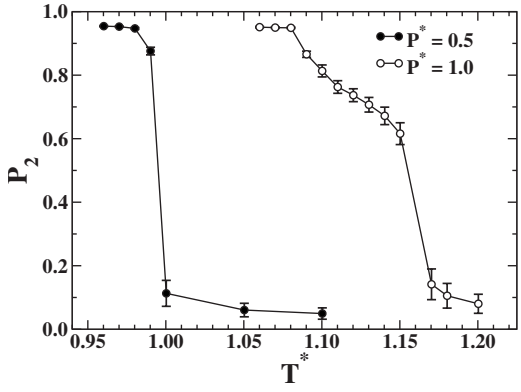

FIG. 1. Orientational order parameter as function of temperature at two pressures for a pure GB fluid with $\kappa=3.0$, $\nu=2$, and $\mu=1$.

this temperature. We have checked that the intermediate state at $T^*=0.99$ is indeed stable by performing extra-long simulation runs. Similar stepwise changes upon lowering the temperature are seen in the average density and internal energy. Altogether, the results in Figs. 1 and 2 suggest the presence of two first-order orientational phase transitions, which are accompanied by a marked decrease of the potential energy and a significant increase of density. To identify the character of the anisotropic phases we present in Fig. 3 results for the correlation functions introduced in Sec. II C at two characteristic temperatures. At $T^*=0.99$, i.e., directly below the first phase transition, the longitudinal function $g_{\parallel}(r_{\parallel})$ exhibits long-ranged oscillations with a period of approximately the particle length ($L_A=3.0\sigma_0$). On the other hand, the transverse functions $g_{\perp}(r_{\perp})$ and $g'_{\perp}(r_{\perp})$ have a rather short-ranged structure, indicating the presence of a Sm_A phase. This becomes different at temperatures below the second phase transition, e.g., at $T^*=0.96$ (see lower part of Fig. 3), where the pronounced structure in the transverse correlations, in particular the split second (first) peak in $g_{\perp}(r_{\perp})$ [$g'_{\perp}(r_{\perp})$] points to Sm_B-like ordering characterized by local hexagonal arrangement of the molecules. We note that this arrangement is also reflected in the *parallel* correlation function [as defined in Eq. (2.10)] within the Sm_B state. Indeed, closer inspection of the lower part of Fig. 3 shows that the first (third, etc.) peak in $g_{\parallel}(r_{\parallel})$ is much smaller than the second (fourth, etc.)

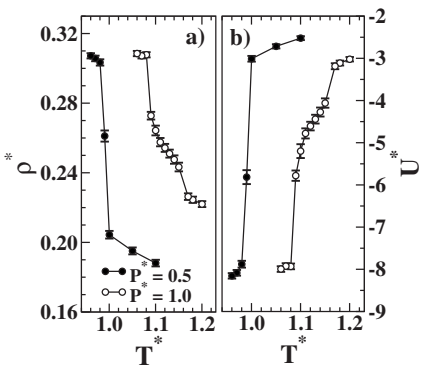

FIG. 2. (a) Average density and (b) internal energy as function of temperature at two different pressures for a pure GB fluid with $\kappa=3.0$.

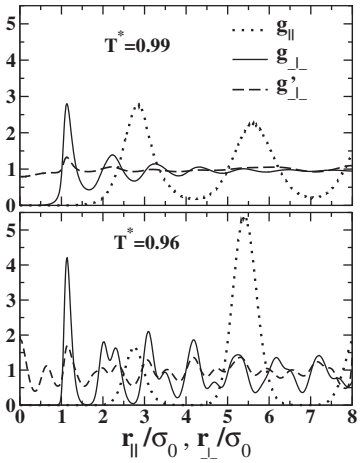

FIG. 3. Correlation functions parallel and perpendicular to the director at two characteristic temperatures for a pure GB fluid with $\kappa=3.0$ ($P^*=0.5$).

peak. The reduction of the first peak reflects that the neighbors of a particle in the two adjacent layers (i.e., $r_{\parallel}\approx L_A$) are somewhat shifted horizontally (i.e., $r_{\perp}\neq 0$). This shift is reversed in the next-nearest layers ($r_{\parallel}\approx 2L_A$), which explains the height of the second peak. Notice that no such shifts appear in the Sm_A phase as reflected by the very similar heights of the first and second peak in the corresponding $g_{\parallel}(r_{\parallel})$ (see top part of Fig. 3).

Whereas the appearance of a Sm_B phase at high densities and low temperatures is a typical feature of GB fluids, the intermediate Sm_A ordering observed in the present study (at $P^*=0.5$) is somewhat surprising in the light of earlier simulations [34,35] with $\nu(\mu)=1(2)$, where such phases have only been observed at higher elongations κ. Instead, these fluids develop nematic ordering in between the isotropic and the Sm_B phase. We note that the present system also displays nematic phases but only at higher pressures (indeed, the increase of nematic phase regions with increasing pressure is a generic feature of GB fluids irrespective of the elongation considered [35]). An example is the pressure $P^*=1.0$ for which the function $P_2(T)$ is shown in Fig. 1. Upon cooling from the isotropic high-temperature state, the system first develops (for $T^*\lesssim 1.15$) nematic ordering as reflected by the smaller values of P_2 (compared to those typical for smectic phases) and the liquidlike behavior of the correlation functions (not shown). Only at temperatures $T^*\lesssim 1.08$ a Sm_B phase becomes stable.

From the appearance of Sm_A and N states as intermediate phases at lower and higher pressures, respectively, we conclude that the effect of increasing the exponent ν from $\nu=1$ (as chosen in the "original" GB fluids) to $\nu=2$ is comparable to the effect of increasing κ previously studied for the "original" system [35]. Indeed, the orientational behavior observed in the present system with $\kappa=3.0$ rather resembles (on a qualitative level) that of original GB molecules with $\kappa \gtrsim 3.2$. Further evidence for this correspondence is that the present system does not display a vapor-liquid critical point within the isotropic phase [47], which does appear in the original GB fluid with $\kappa=3.0$, but not for more elongated

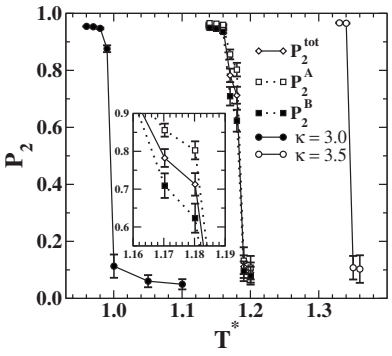

FIG. 4. Orientational order parameters as a function of temperature for mixture I ($P^*=0.5$). Plotted are the data for the pure A and B systems, respectively, the *total* order parameter of the mixture, and the values of each component. The inset shows the data for intermediate temperatures on an expanded scale.

particles ($\kappa \gtrsim 3.2$) where the critical point falls below the I-Sm$_B$ coexistence line [35].

B. Weak bidispersity: Mixture I

We now turn to the phase behavior of GB mixtures, starting with system I (see Table I) where the B component consist of the particles discussed in Sec. III A (that is, $\kappa_B=3.0$). Also, compared to the other mixtures studied in this work, system I is characterized by the largest value of the parameter q, that is, by the smallest degree of bidispersity.

In all of the subsequent simulations, the pressure is fixed at $P^*=0.5$. Results for the orientational parameters as functions of the temperature are given in Fig. 4 where the data for the pure B system (left-most curve) equal those plotted in Fig. 1. The right-most curve corresponds to the pure A fluid, which develops orientational ordering at temperatures much higher than the corresponding ones in the pure B fluid. This shift may be understood as a consequence of the higher elongation of the A particles ($\kappa_A=3.5$). Furthermore, analysis of the corresponding correlation functions (not shown) reveals that the isotropic phase in the pure A fluid directly transforms into a Sm$_B$ phase, indicating that the chosen pressure is too low to stabilize the less-ordered Sm$_A$ phase observed in the pure B fluid at the same pressure (and $T^* \approx 0.99$, see Sec. III A).

Considering now the true A-B mixture, the jumps in the total order parameter P_2^{tot} (see Fig. 4) suggest the presence of *two* orientational phase transitions at $T^* \approx 1.19$ and $T^* \approx 1.16$. These temperatures are between the typical transition temperatures of the pure systems, reflecting that the presence of less elongated particles *hinders*, to some extent, the ordering of the larger component. We also see from the species-resolved order parameters P_2^a that the two components develop orientational ordering simultaneously. The actual values of these parameters indicate a somewhat lower degree of ordering of the (less elongated) B particles at intermediate temperatures ($1.16 \lesssim T^* \lesssim 1.19$), reflecting a greater orientational freedom of this species. On the other hand, the low-temperature range ($T^* \lesssim 1.6$) is characterized by nearly equal values of P_2^A and P_2^B.

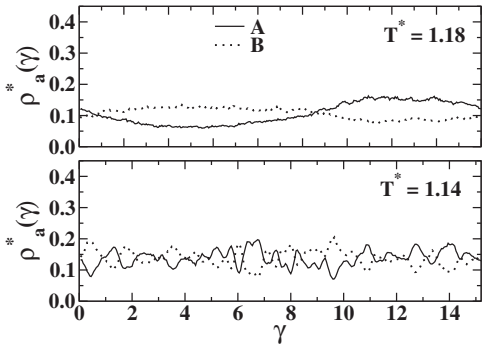

FIG. 5. Density profiles in mixture I ($a=A,B$) at two characteristic temperatures. γ denotes the Cartesian direction along which the system becomes inhomogeneous ($\gamma=x,y,z$).

To see whether the anisotropic states detected from Fig. 4 are indeed *single* phases or rather *demixed* states, which would imply coexistence of two phases with different composition, we consider in Fig. 5 results for the species-resolved density profiles defined in Eq. (2.13). At a temperature below the first phase transition (e.g., $T^*=1.18$, corresponding to a total density of $\rho_{\text{tot}}^* \approx 0.21$) the density profiles exhibit two weak oscillations which may indicate some *tendency* of the two species to segregate into different regions in the simulation box. However, the actual amplitude of these oscillations and the resulting composition "differences" within the box regions, is too small ($|\rho_A^* - \rho_B^*| \leq 0.06$) to infer to the presence of a true demixed state. We thus consider the present state as a mixed state, and take the weak oscillations as a hint that there *might be* a demixing transition at higher pressures.

Corresponding correlation functions characterizing the structure of the A and B particles in this mixed anisotropic phase are plotted in Fig. 6.

The oscillations in $g_{\parallel}^{AA}(r_{\parallel})$ together with the liquidlike transverse structure visible from $g_{\perp}^{AA}(r_{\perp})$ indicate that the A particles form a Sm$_A$ phase, with the layer spacing corre-

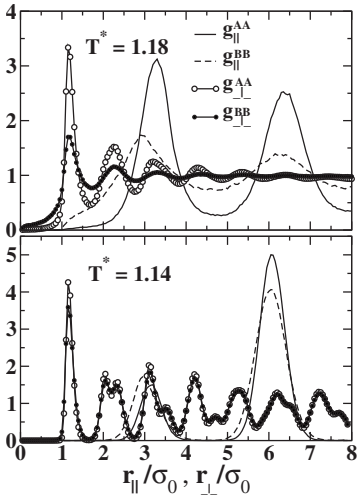

FIG. 6. Correlation functions parallel and perpendicular to the director evaluated for mixture I at the same temperatures appearing in Fig. 5.

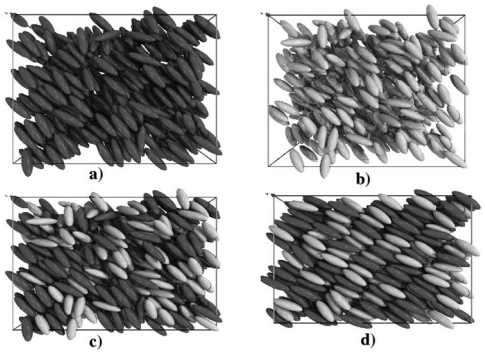

FIG. 7. Simulation "snapshots" corresponding to the temperatures considered in Fig. 5. (a) A particles at $T^*=1.18$, (b) B particles at $T^*=1.18$, (c) full system at $T^*=1.18$, (d) full system at $T^*=1.14$.

sponding roughly to the particle length ($L_A=3.5\sigma_0$). This is particularly interesting given that the pure A fluid does not have a Sm_A phase at the pressure considered. Results for $g_{\parallel}^{BB}(r_{\parallel})$ and $g_{\perp}^{BB}(r_{\perp})$ are less conclusive, but might be interpreted either as a nematic ordering of the B particles with strong short-ranged correlations or as a weak Sm_A-like ordering of this species (note that the pure B system does indeed have a Sm_A phase at $P^*=0.5$). Thus, we consider a mixed anisotropic phase where the less elongated B particles behave in a more or less fluidlike manner (with, consequently, smaller degree of alignment) within the layered structure formed by the A particles. This picture is confirmed by simulation "snapshots" taken at $T^*=1.18$, which are presented in Figs. 7(a)–7(c). Specifically, Figs. 7(a) and 7(b) show separately the structuring of the molecules of each species, whereas Fig. 7(c) reveals the mixed nature of the full system.

A second change of the mixture's behavior occurs at low temperatures. As a representative temperature we consider $T^*=1.14$ (corresponding to a total density of $\rho_{\mathrm{tot}}^*\approx 0.28$). At this temperature, the density profiles plotted in Fig. 5 (bottom) are almost constants suggesting that the system is again in a mixed state. The same picture emerges from the snapshot shown in Fig. 7(d). Corresponding correlation functions indicate a Sm_B-type ordering of *both*, the A and the B particles with the layer spacing being dominated by the A species. Thus, although there are two competing length scales in the system (L_A and $L_B=0.86\times L_A$), the resulting frustration is not strong enough at $q=0.86$ to prevent a mixed smectic phase. This finding is consistent with earlier MD simulation results by Bemrose *et al.* [37] who investigated the same mixture (with the same exponents ν and μ) at a fixed total density of $\rho_{\mathrm{tot}}^*=0.25$ in a microcanonical ensemble. At low temperatures, where the pressure becomes comparable to the one considered here, they found mixed Sm_B states. On the other hand, at higher temperatures (and corresponding pressures much larger than that considered here) they observed I-N coexistence instead of the Sm_A-like phases found in the present work.

C. Moderate bidispersity: Mixture II

We now turn to the second mixture characterized by $\kappa_{A(B)}=2.5(2.0)$ (see Table I) and a resulting bidispersity parameter of $q=0.80$. The main question is whether the increased bidispersity (as compared to that in mixture I) can drive fractionation *in spite* of the reduced elongation of the particles.

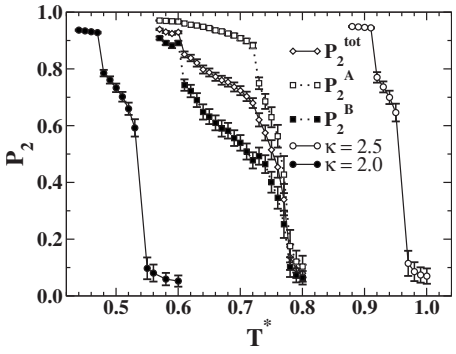

FIG. 8. Orientational order parameters as a function of temperature for mixture II ($P^*=0.5$). Labels are the same as in Fig. 4.

The ordering behavior of the corresponding pure fluids is illustrated in Fig. 8, where we have plotted all the functions $P_2(T)$ characterizing this system. Both pure fluids display two orientational phase transitions upon cooling, with the order parameter functions being essentially just shifted from each other. The first transition leads from the isotropic phase into a state with nematic ordering, as indicated by the corresponding correlation functions (not shown) and by the relatively low values of P_2. Further cooling of the pure fluids then yields a second phase transition from the nematic into a Sm_B phase. Thus, there is no intermediate Sm_A phase, which may be traced back to the quite small elongation of the particles considered ($\kappa=2.0/2.5$).

Compared to the pure systems the order parameter functions for the mixture, and the corresponding behavior of the total density and potential energy plotted in Fig. 9 indicate more complex fluid-fluid phase behavior. Indeed, on cooling from high temperatures one observes a first significant increase of P_2^{tot} and the P_2^a (accompanied by a corresponding decrease of the total internal energy, U_{tot}^*) at $T^*\approx 0.77$, followed by two first-order phase transitions at $T^*\approx 0.73$ and $T^*\approx 0.60$.

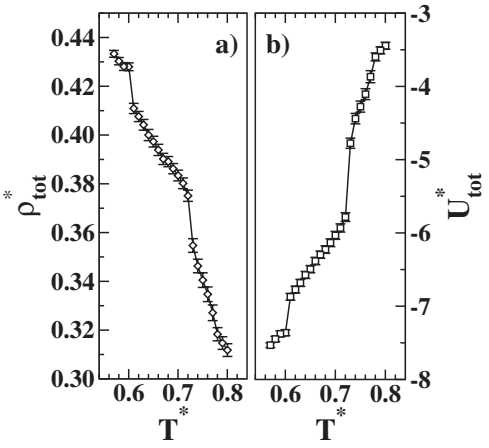

FIG. 9. (a) Average total density and (b) total internal energy as a function of temperature for mixture II.

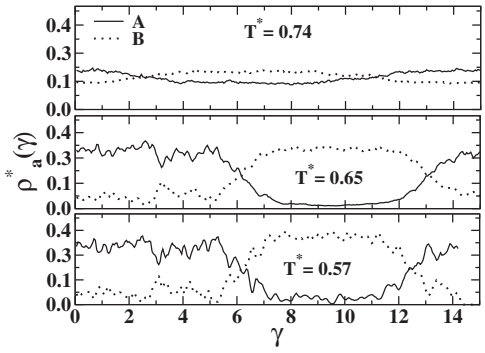

FIG. 10. Density profiles in mixture II at three characteristic temperatures.

In the first temperature range ($0.73 \lesssim T^* \lesssim 0.77$), the system is still essentially mixed. This can be seen from the density profiles plotted at the exemplary temperature $T^*=0.74$ in the upper part of Fig. 10, or, more directly, from the corresponding simulation "snapshot" presented in Fig. 11(a). Moreover, corresponding correlation functions plotted in Fig. 12 indicate nematic ordering of both species, which is consistent with the relatively small order parameter $0.3 \lesssim P_2^A$, $P_2^B \lesssim 0.6$ characterizing this temperature range (see Fig. 8). Thus, we are facing a mixed nematic state. We note that stable nematic mixtures have previously been observed at significantly higher pressures in *NPT*-Gibbs ensemble Monte Carlo (GEMC) simulations of Mills *et al.* [38] who focused, however, on properties of the *I-N* coexistence.

Cooling the system toward temperatures below the second phase transition (located at $T^* \approx 0.73$) yields a further increase of the total orientational order as measured by the parameter P_2^{tot}. Closer inspection of Fig. 8 reveals that this concerns particularly the longer *A* particles. At the same time, the system *demixes* into one phase consisting nearly exclusively of *A* particles, and the other one being dominated by *B* particles, as revealed by the density profiles and snapshots presented in Fig. 10 (middle) and Fig. 11(b), respectively, for the exemplary temperature $T^*=0.65$. Given that the orientational phase transitions are of first order, the appearance of demixing implies that there must exist a *triple point* (with triple temperature and pressure close to $T^*=0.73$ and $P^*=0.5$, respectively), where the mixed nematic phase coexists with two, more strongly ordered, phases characterized by markedly different compositions and different orientational structure. A precise localization of such triple points (as well as of other true coexistence points) is not possible within the present *NPT*-MD approach since we did not calculate the chemical potentials μ_A and μ_B.

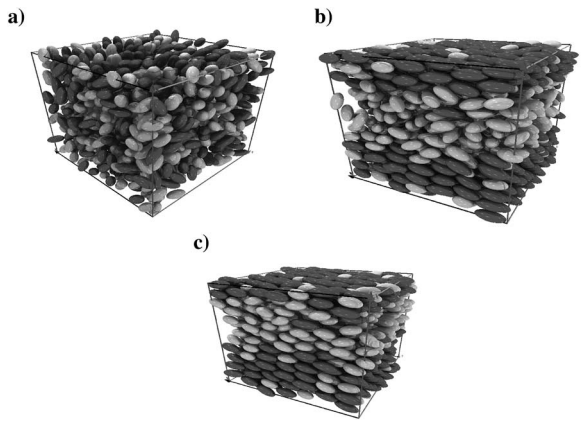

FIG. 11. Simulation "snapshots" corresponding to the temperatures considered in Fig. 10. (a) $T^*=0.74$, (b) $T^*=0.65$, (c) $T^*=0.57$.

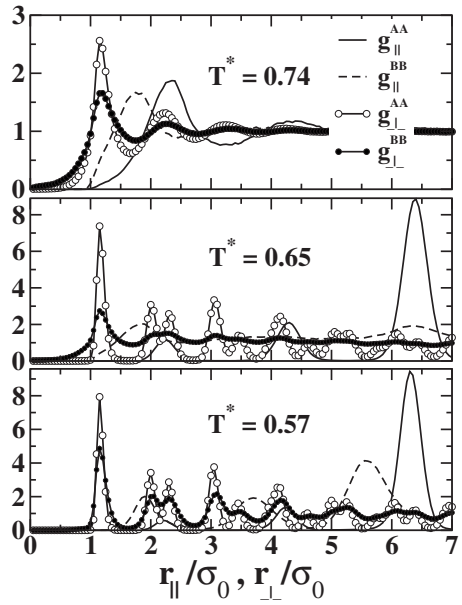

FIG. 12. Correlation functions parallel and perpendicular to the director evaluated for mixture II at the same temperatures appearing in Fig. 10.

A further indication of the global demixing at temperatures $T^* \lesssim 0.73$ are the fairly large differences between P_2^B and $P_2^A > P_2^B$ visible from Fig. 8 (note that due to the pronounced demixing, the two species order parameters can be considered as an estimate of the *total* order parameters in each demixed phase). These differences in the degree of orientational order are accompanied by differences in the translational structure. Indeed, as seen from the corresponding correlation functions in Fig. 12, the *A* particles form a Sm_B state, whereas the less elongated *B* particles rather show

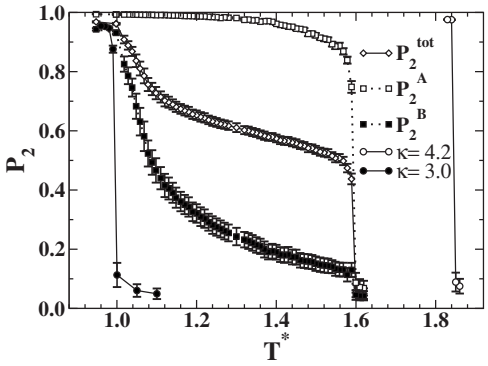

FIG. 13. Orientational order parameters as a function of temperature for mixture III ($P^*=0.5$). Labels are the same as in Fig. 4.

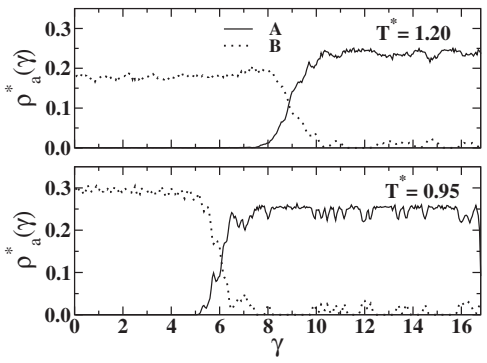

FIG. 14. Density profiles in mixture III at two characteristic temperatures.

nematic ordering. We note that some evidence for global demixing has also been found in the *NPT*-GEMC simulations of Mills *et al.* [38] who did not, however, characterize the demixed phases and their structure as a function of temperature.

Irrespective of the demixing behavior it is interesting to note that the temperature range $|\Delta T_N^*|$, in which mixture II is (at least partially) in a nematic state ($|\Delta T_N^*| \approx |0.6-0.77| = 0.17$), is significantly *larger* than the nematic range in the pure systems at $\kappa=2.0$ or $\kappa=2.5$ ($|\Delta T^*| \approx 0.03$). This growth of $|\Delta T_N^*|$ is consistent, on a qualitative level, with several experimental observations indicating an increase of the stability range of nematic phases upon mixing one type of elongated molecule with another type [12,13].

Finally, at the lowest temperatures considered ($T^* \lesssim 0.6$) the system is nearly fully demixed as reflected by the density profile plotted in the bottom part of Fig. 10 and the corresponding snapshot in Fig. 11(c). Each of the two phases displays Sm_B-like ordering, which is seen most clearly from the correlation functions plotted in the bottom part of Fig. 12. Notice, in particular, the split second peak (typical for Sm_B states) appearing in the perpendicular correlations of the *B* particles which is absent at the intermediate temperature $T^*=0.65$ (middle part of Fig. 12). Due to the demixing, the low-temperature behavior of mixture II differs markedly from that of mixture I, which forms a *mixed* Sm_B phase as discussed at the end of Sec. III B. We understand this difference as a consequence of the somewhat larger degree of bidispersity in mixture II ($q=0.80$) [as compared to mixture I ($q=0.86$)], which disfavors formation of smectic layers accommodating molecules of lengths (as it is the case in mixture I).

D. Strong bidispersity: Mixture III

We finally turn to mixture III which is characterized by both, longer molecules than the ones involved in mixture II discussed before, and an even larger degree of bidispersity ($q=0.71$). The pure *B* species ($\kappa_B=3.0$) involved in mixture III has already been considered in Sec. III A; this fluid exhibits an *I*-Sm_A transition followed by a Sm_A-Sm_B transition upon cooling at $P^*=0.5$. On the other hand, the pure *A* fluid ($\kappa_A=4.2$) transforms directly from the isotropic into a Sm_B phase, similar to the pure $\kappa=3.5$ fluid discussed at the beginning of Sec. III B. This may be seen from the corresponding order parameter plotted in Fig. 13, which "jumps" from negligible values in the isotropic phase directly to the (nearly maximal) value $P_2 \approx 0.98$.

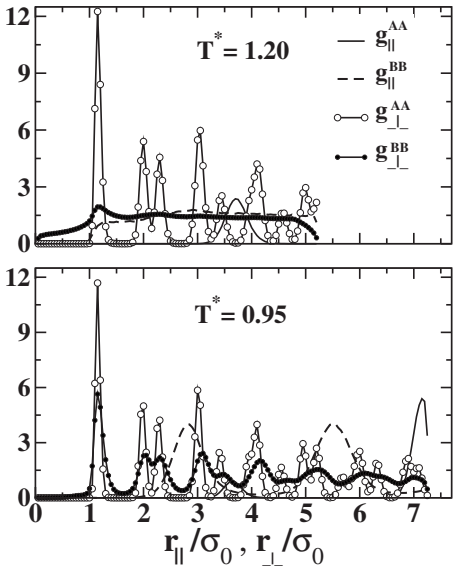

FIG. 15. Correlation functions parallel and perpendicular to the director evaluated for mixture II at the temperatures considered in Fig. 14.

In view of the marked length differences characterizing mixture III one would expect demixing scenarios to become even more dominant as compared to the case $q=0.80$ discussed in Sec. III C. That this is indeed the case, can be seen from the order parameters in the true mixture (see Fig. 13), as well as from the density profiles plotted in Fig. 14. Clearly, the system demixes *immediately* as soon as orientational ordering starts to develop at $T^* \approx 1.6$ (we have explicitly checked that this effect remains with the larger system size of $N=4000$). Below the coupled orientational-demixing phase transition there is a fairly large temperature range ($1.0 \lesssim T^* \lesssim 1.6$) where the *B* particles (in other words, the particles in the *B*-dominated phase) are only weakly aligned, whereas the *A*-dominated phase is characterized by very large values of P_2^A. Corresponding correlation functions plotted in Fig. 15 (top) suggest that the *A* particles form a Sm_B state, whereas the *B* particles are only very weakly correlated reflecting a nematic structure in this (*B*-dominated) phase. Thus, although the system is globally demixed, the *B* particles behave very different compared to a pure *B* fluid with $\kappa_B=3.0$. Moreover, we also see that the range of the *partially* nematic state $|\Delta T_N^*|$ (as defined in Sec. III C) has again increased. Finally, at the lowest temperatures considered, both demixed phases have Sm_B structure similar to what we have observed in mixture II (see Fig. 11).

IV. CONCLUSIONS

In this paper we have used constant-pressure MD simulations in order to explore the phase behavior of dense, binary LC mixtures of prolate GB ellipsoids characterized by differ-

TABLE II. GB parameters of mixture I ($q=0.86$) [37].

	AA	*BB*	*AB*	*BA*
χ_{ab}	0.849	0.800	0.824	0.824
χ'_{ab}	0.666	0.666	0.6662	0.6662
$\epsilon_{ab}/\epsilon_{BB}$	1.103	1.0	1.050	1.050
α_{ab}	1.0	1.0	1.015	0.985
α'_{ab}	1.0	1.0	1.011	0.989

TABLE IV. GB parameters of mixture III ($q=0.71$) [39].

	AA	*BB*	*AB*	*BA*
χ_{ab}	0.893	0.800	0.845	0.845
χ'_{ab}	0.666	0.666	0.6665	0.6665
$\epsilon_{ab}/\epsilon_{BB}$	1.175	1.0	1.085	1.085
α_{ab}	1.0	1.0	1.028	0.973
α'_{ab}	1.0	1.0	1.019	0.982

ent lengths (with length ratios $q=0.86$, 0.80, and 0.71) and equal diameters. The main objective was to achieve a deeper understanding of the interplay between orientational ordering transitions familiar from one-component GB fluids, on the one hand, and macroscopic demixing transitions ("fractionation"), on the other hand. Our key results can be summarized as follows.

(1) The "driving forces" for fractionation are a sufficiently pronounced length difference between the particles of the two species (i.e., small values of q) combined with sufficiently low temperatures. Indeed, at high temperatures all systems considered are in a mixed isotropic state whereas the behavior upon cooling strongly depends on q. At $q=0.86$ the systems stay in a mixed state even at the lowest temperatures investigated, where the overall structure is that of a Sm_B phase (with the layer spacing being determined by the length of the longer particles). On the contrary, the system with $q=0.71$ demixes immediately when orientational order (into a demixed Sm_B-N state) starts to develop, the low-temperature state is then a demixed Sm_B-Sm_B phase. In the intermediate case $q=0.80$ we observe a three-step ordering and demixing scenario on cooling the system from high temperatures.

(2) For all q considered the mixture's phase behavior is more complex compared to that of the corresponding pure systems and cannot just be viewed as an interpolation of the latter. In particular, each component can behave different from its pure counterpart even when the system is globally demixed. An interesting example is the (nematic) behavior of the B particles in mixture III under conditions where the pure B fluid develops smectic ordering.

(3) For the two mixtures where fractionation takes place ($q=0.80, 0.71$) the temperature range $|\Delta T_N^*|$, in which the system is (at least partially) in a nematic state is significantly *larger* than the nematic range in the pure systems. Thus, bidispersity yields a growth of the parameter region where nematic states are stable, in qualitative agreement with experimental observations in organic LC compounds.

TABLE III. GB parameters of mixture II ($q=0.80$) [38]

	AA	*BB*	*AB*	*BA*
χ_{ab}	0.724	0.600	0.659	0.659
χ'_{ab}	0.666	0.666	0.660	0.660
$\epsilon_{ab}/\epsilon_{BB}$	1.316	1.0	1.147	1.147
α_{ab}	1.0	1.0	1.048	0.954
α'_{ab}	1.0	1.0	1.030	0.971

(4) Compared to earlier simulations involving the same model parameters, the present *NPT*-MD simulations provide insight to the system's behavior at lower pressures, where smectic (A or B) rather than nematic ordering occurs. Our results show that this difference in thermodynamic conditions yields qualitatively, interesting demixing phenomena not occurring at higher pressures.

It is clear that the present study, where we have focused on one particular pressure, cannot give a complete picture of the mixture's phase behavior. For example, we have not touched the low density region where liquid-vapor transitions (which may be accompanied by demixing transitions) can be expected to take place. Another open issue is the precise *location* of the phase transitions both at high and low densities, which requires free energy methods to be employed. Also, one would like to understand the *interfacial structure* at the first-order orientational phase transitions of the mixture. Work in these directions is currently under way. Finally, we would like to point out that we do not expect the temperature-driven demixing scenarios observed in the present work to be restricted to GB mixtures; indeed, qualitatively similar behavior is likely to occur in any LC model mixture combining repulsive and attractice interactions. Examples are the mixtures of attractive rods considered in Ref. [22] (where microphase separation has already been seen) or the Lennard-Jones "sticks" recently suggested in Ref. [48].

The authors thank M. Wilson for his help in calculating the transversal and perpendicular correlation functions. One of the authors (J.A.M.R.) acknowledges support from CONACYT (Contract No. 162761). Two of the authors (E.D.H., J.A.M.R.) gratefully acknowledge financial support from CONCYT-Mexico. Furthermore, one of the authors (S.H.L.K.) thanks the Deutsche Forschungsgemeinschaft for funding through the Sonderforschungsbereich 448 "mesoscopically structured composites" and the Emmy-Noether Programme.

APPENDIX: SYSTEM PARAMETERS

As seen from the model equations presented in Sec. II A there is a considerable amount of parameters (in addition to the geometric ones) defining the GB mixture. To start with, there are the quantities χ_{ab} and α_{ab}, which follow from the lengths and breadths according to Eqs. (2.4) and (2.5). Next, there are the interaction parameters ϵ_{ab} [see Eq. (2.6)]. In this work we use $\epsilon_{BB}=1.0$ as a reference energy scale, and the values for $\epsilon_{AA}/\epsilon_{BB}$ are taken from Refs. [37–39]. The cross

parameters $\epsilon_{AB(BA)}$ then follow from the Lorentz-Berthelot mixing rule, i.e., $\epsilon_{AB(BA)}/\epsilon_{BB}=\sqrt{\epsilon_{AA}\epsilon_{BB}}/\epsilon_{BB}=\sqrt{\epsilon_{AA}/\epsilon_{BB}}$. As to the exponents ν and μ appearing in Eq. (2.6), we follow the earlier simulations [37–39] in setting $\nu=2$ and $\mu=1$ irrespective of the component considered (this differs from the choice originally suggested by Gay and Berne [33] where $\nu=1$, $\mu=2$). We further set the attraction ratios $\kappa'_{AA}=\kappa'_{BB}=5.0$ [see Eq. (2.9)] implying that the attraction in a side-by-side configuration of two A (B) particles is 5 times larger than in a corresponding end-to-end configuration. This choice implies $\chi'_{AA}=\chi'_{BB}=0.666$ [see Eq. (2.9)]. Values for the remaining (six) quantities $\chi'_{AB(BA)}$ and α'_{ab} are taken from Refs. [37–39]. A summary of the parameters employed in the present simulations is given in Tables II–IV.

[1] F. Reinitzer, Monatsh. Chem. **9**, 421 (1888).
[2] O. Lehmann, Z. Phys. Chem. **4**, 462 (1889).
[3] H. Zocher, Z. Anorg. Chem. **174**, 91 (1925).
[4] F. C. Bawden, N. W. Pirie, J. D. Bernal, and I. Fankuchen, Nature (London) **138**, 1051 (1936).
[5] P. G. De Gennes and J. Prost, *The Physics of Liquid Crystals*, 2nd ed. (Oxford University Press, Oxford, 1995).
[6] L. Onsager, Ann. N. Y. Acad. Sci. **51**, 627 (1949).
[7] M. P. Allen, G. T. Evans, D. Frenkel, and B. M. Mulder, Adv. Chem. Phys. **86**, 1 (1993).
[8] P. Pasini, C. Zannoni, and S. Zumer, *Computer Simulations of Liquid Crystals and Polymers* (Kluwer, Dordrecht, 2005).
[9] C. M. Care and D. J. Cleaver, Rep. Prog. Phys. **68**, 2665 (2005).
[10] P. G. Bolhuis and D. Frenkel, J. Chem. Phys. **106**, 666 (1997).
[11] S. C. McGrother, A. Gil-Villegas, and G. Jackson, Mol. Phys. **95**, 657 (1998).
[12] W. H. de Jeu, L. Longa, and D. Demus, J. Chem. Phys. **84**, 6410 (1986).
[13] J. C. Hwang, S. C. Liang, K. H. Liang, and J. R. Chang, Liq. Cryst. **26**, 925 (1999).
[14] M. B. Sied, D. O. López, J. Ll. Tamarit, and M. Barrio, Liq. Cryst. **29**, 57 (2002).
[15] M. M. Naoum, R. I. Nessim, and T. Y. Labeeb, Liq. Cryst. **27**, 889 (2000).
[16] P. A. Buining and H. N. W. Lekkerkerker, J. Phys. Chem. **97**, 11510 (1993).
[17] M. P. B. van Bruggen, F. M. van der Kooij, and H. N. W. Lekkerkerker, J. Phys.: Condens. Matter **8**, 9451 (1996).
[18] S. Iijima, Nature (London) **138**, 1051 (1991).
[19] H. N. W. Lekkerkerker, Ph. Coulon, R. Van Der Haegen, and R. Deblieck, J. Chem. Phys. **80**, 3427 (1984).
[20] T. Odijk and H. N. W. Lekkerkerker, J. Phys. Chem. **89**, 2090 (1985).
[21] G. J. Vroege and H. N. W. Lekkerkerker, J. Phys. Chem. **97**, 3601 (1993).
[22] A. Richter and T. Gruhn, J. Chem. Phys. **125**, 064908 (2006).
[23] X. Zhou, H. Chen, and M. Iwamoto, J. Chem. Phys. **120**, 1832 (2004).
[24] J. M. Polson and E. E. Burnell, Chem. Phys. Lett. **281**, 207 (1997).
[25] T. Koda and H. Kimura, J. Phys. Soc. Jpn. **63**, 984 (1994).
[26] G. Cinacchi, E. Velasco, and L. Mederos, J. Phys.: Condens. Matter **16**, S2003 (2004).
[27] G. Cinacchi, L. Mederos, and E. Velasco, J. Chem. Phys. **121**, 3854 (2004).
[28] S. Varga, K. R. Purdy, A. Galindo, S. Fraden, and G. Jackson, Phys. Rev. E **72**, 051704 (2005).
[29] K. R. Purdy, S. Varga, A. Galindo, G. Jackson, and S. Fraden, Phys. Rev. Lett. **94**, 057801 (2005).
[30] R. van Roij, B. Mulder, and M. Dijstra, Physica A **261**, 374 (1998).
[31] G. Cinacchi, Y. Martinez-Raton, L. Mederos, and E. Velasco, J. Chem. Phys. **124**, 234904 (2006).
[32] W. Maier and A. Saupe, Z. Naturforsch. A **14A**, 882 (1959); **15A**, 287 (1960).
[33] G. J. Gay and B. J. Berne, J. Chem. Phys. **74**, 3316 (1981).
[34] E. de Miguel, L. Rull, M. K. Chalam, and K. E. Gubbins, Mol. Phys. **74**, 405 (1991).
[35] J. T. Brown, M. P. Allen, E. Martin del Río, and E. de Miguel, Phys. Rev. E **57**, 6685 (1998).
[36] D. J. Cleaver, C. M. Care, M. P. Allen, and M. P. Neal, Phys. Rev. E **54**, 559 (1996).
[37] R. A. Bemrose, C. M. Care, D. J. Cleaver, and M. P. Neal, Mol. Phys. **90**, 625 (1997).
[38] S. J. Mills and D. J. Cleaver, Mol. Phys. **98**, 1379 (2000).
[39] S. J. Mills, C. M. Care, P. M. Neal, and D. J. Cleaver, Mol. Cryst. Liq. Cryst. **330**, 423 (1999).
[40] M. P. Allen and D. J. Tildesley, *Computer Simulation of Liquids* (Academic, London, 1987).
[41] E. Díaz-Herrera, G. Ramirez-Santiago, and J. A. Moreno-Razo, Phys. Rev. E **68**, 061204 (2003).
[42] E. Díaz-Herrera, J. A. Moreno-Razo, and G. Ramirez-Santiago, Phys. Rev. E **70**, 051601 (2004).
[43] E. Díaz-Herrera, G. Ramirez-Santiago, and J. A. Moreno-Razo, J. Chem. Phys. **123**, 184507 (2005).
[44] T. Gruhn and M. Schoen, Phys. Rev. E **55**, 2861 (1997).
[45] J. Billeter and R. Pelcovitz, Comput. Phys. **12**, 440 (1998).
[46] R. Eppenga and D. Frenkel, Mol. Phys. **52**, 1303 (1984).
[47] E. Guzman, J. A. Moreno-Razo, and E. Díaz-Herrera (unpublished).
[48] F. J. Vesely, J. Chem. Phys. **125**, 214106 (2006).